光学学报

片上集成人工微结构光场调控(特邀)

王艳春[1]，张跃变[1*]，程化[1**]，陈树琪[1,2***]

[1]南开大学物理科学学院，泰达应用物理研究院，弱光非线性光子学教育部重点实验室，天津 300071；

[2]山西大学极端光学协同创新中心，山西 太原 030006

摘要　光学元件的小型化与集成化一直是光场调控和集成光学领域的研究重点与难点之一。光学人工微结构具有在亚波长尺度上灵活调控光场振幅、偏振、相位、频率等属性的能力。通过与片上光波导或微腔集成，人工微结构可以为实现更紧凑的片上集成光子学器件以及更精确、更丰富的光场调控提供新的解决方案和更多的可能性。本文依据片上集成人工微结构在不同环节中调控的光场类型的差异，将其分成三类进行了讨论。介绍了基于不同设计原理的片上集成人工微结构在自由空间光入射耦合、波导模式面内调控以及离片辐射场调控方向的研究进展，并对该领域的部分新兴方向进行了展望。

关键词　人工微结构；超构表面；光场调控；集成光学；微纳光学

中图分类号　O436　　**文献标志码**　A　　**DOI**：10.3788/AOS240429

1　引　　言

光是重要的能量载体和信息载体，在人类的日常生活中发挥着不可替代的作用。光场的主要信息可由它们的振幅、相位、频率、偏振等少数几个属性维度来描述。如何更加灵活有效地调控这些光场维度一直是光学与光子学领域研究的热点之一。另一方面，随着科技的发展，“摩尔定律”逐渐失效，传统的电子芯片在性能提升方面面临着越来越大的挑战。光子相对于电子有更快的传输速率、更高密度的信息承载能力以及独特的并行处理能力，因此，用光学元件部分或全部代替电子元件有望解决传统电子芯片所面临的诸多问题。但是传统的光学元件一般体积较大、质量较重，因此，将多个光学元件小型化并集成到同一个芯片上是未来光芯片发展的重要趋势。在微纳光学和集成光学[1-2]领域，怎样用面积尽量小的光芯片实现尽量多的光学功能一直是研究热点和难点。光学人工微结构(又被称为“超构原子”)[3]是一种尺寸在亚波长量级的人造微纳结构，它可以与光场发生共振，在极小的体积内增强光与物质的相互作用，从而显著改变光场的原有状态，为光学元件的小型化和集成化提供了强有力的工具。同时，光学人工微结构还能实现一些利用自然材料难以实现的新颖功能，比如隐身斗篷[4-5]、零折射率材料[6-7]、双曲超材料[8-9]等。将光学人工微结构在二维表面上进行有序排列便构成了光学超构表面[10-16]，通过改变其中人工微结构的尺寸或排列方式便可以灵活调控光场的偏振、相位、振幅等属性。近年来，研究者们基于超构表面实现了大量新颖的功能和应用，比如近完美吸收器[17-19]、偏振转换器[20-22]、光束偏折器[23-26]、超构透镜[27-31]、超全息[32-34]、结构色[35-38]、编码超构表面[39]、非线性超构表面[40-46]等。这些超构表面不仅为传统光学元件的小型化和集成化提供了切实有效的解决方案，而且提供了更加多样化的光场调控手段和更加丰富的光与物质相互作用过程。然而，目前的超构表面大多都是基于对自由空间光场的调控，并且每个超构表面往往只能实现单个或少数几个功能，距离真正实现大规模的光子器件集成还有很长的路要走。

为了进一步实现更紧凑、功能更丰富的光子芯片，近几年研究者们开始将光学人工微结构与片上光波导或光学微腔集成在一起，进一步拓展了人工微结构的应用范围[47-51]。人工微结构由于其亚波长尺寸的尺度优势和独特的共振特性，可以成为连接自由空间光场与片上导波模式的桥梁，也可以用来对片上导波模式进行调控，从而为未来片上集成光子器件和集成光芯片的设计打开新的广阔空间。如图 1 所示，片上集成人工微结构可以根据它们调控的光场类型分为三类。第一类是可以将自由空间光模式耦合到波导中并转化

收稿日期：2024-01-02；**修回日期**：2024-01-22；**录用日期**：2024-01-29；**网络首发日期**：2024-02-20

基金项目：国家重点研发计划(2021YFA1400601，2022YFA1404501)、国家杰出青年科学基金(11925403)、国家自然科学基金(12122406，12192253)

通信作者：*ybzhang@nankai.edu.cn；**hcheng@nankai.edu.cn；***schen@nankai.edu.cn

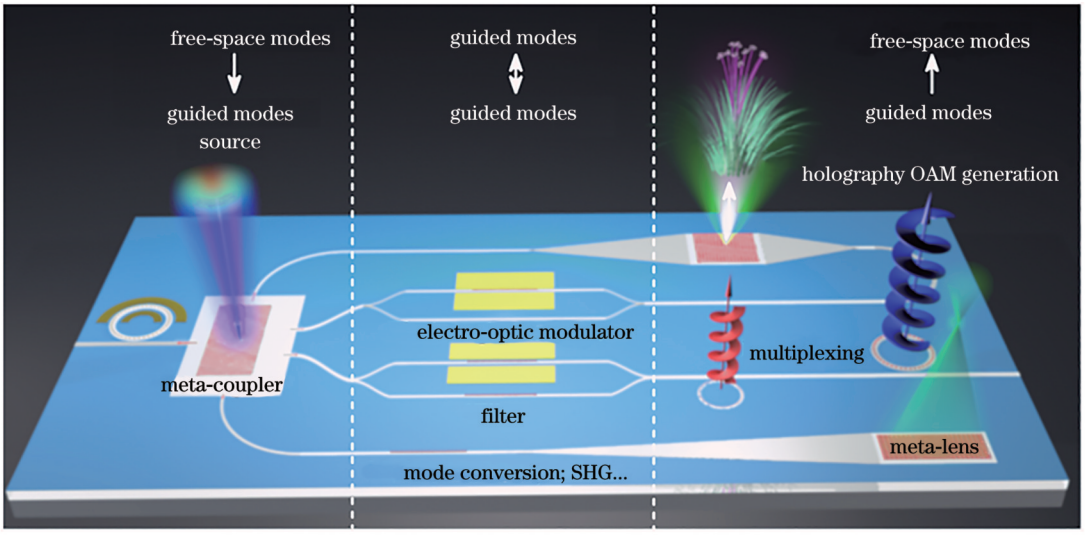

图 1　基于片上集成人工微结构的光场调控示意图

Fig. 1　Schematic of optical field manipulation based on on-chip integrated artificial microstructures

为特定导波模式的“超耦合器”。相比于传统的光栅耦合器，基于人工微结构的超耦合器可以实现更多样、更复杂的功能，比如实现波长、偏振的多路复用[52-54]，或实现特定导波模式的激发[55]。第二类是可以在芯片平面内对片上束缚光场进行调控的“面内调控器”，可以实现导波模式的面内聚焦[56]、不同导波模式间的相互转化[57-58]、滤波[59]、片上非线性谐波生成[60]等功能。并且片上集成人工微结构还可以与电光调制器等动态调控方案结合在一起，进一步提升调制器的尺寸、带宽等性能[61]。第三类是可以将导波重新转化为自由空间波的“导波驱动超构表面”。基于人工微结构强大的光场调控能力，波导和微腔中的片上导波模式可以转化为能够在自由空间中传播的复杂光场模式，实现全息成像[62]、涡旋光束生成[63-64]、光束聚焦[65]、光束偏折[66]等波前调控功能。出射光场的偏振、振幅、相位、轨道角动量等属性理论上都可以任意调控，从而为虚拟现实、增强现实、信息加密与多路复用等应用提供了新的解决方案。

片上集成人工微结构为光场调控和微纳光子学器件的研究注入了新的活力，正在迎来它的技术爆发期。本文将系统介绍以上三种类型的片上集成人工微结构，从它们的基本原理、设计方法、功能应用等方面概述该领域的研究现状与最新进展，并展望该领域的部分新兴方向，以期为该领域的研究者们提供有用的指导和启发。

2　基于片上集成人工微结构的入射耦合调控

在光子学和集成光学领域，自由空间光与波导的耦合过程一直是一个备受关注的研究课题。光的自由空间传输和波导内传输具有不同的特性和规律，而将自由空间光有效地耦合入片上光波导或微腔，对于实现高效的光子器件和集成光路具有重要意义。早期，研究者们多是通过光纤或棱镜来将光耦合到波导或微腔里[67-68]，然而，这种耦合方案往往需要精确的对准操作和复杂的实验光路，大大限制了集成光路的应用场景。另一种常见的方法是光栅耦合法[69-70]，然而，光栅耦合一般需要入射光以特定角度入射，不能有效地用于发散光束的耦合。且光栅耦合往往对入射光的偏振和波长比较敏感，不利于光子集成。人工微结构可以在亚波长尺度与光场发生共振耦合，因此可以通过结构的设计减轻其对入射光的角度、波长和偏振的依赖，可以实现对自由空间光更高效的入射耦合和更灵活的调控。

将自由空间光定向耦合到片上光波导或微腔中对于无线光通信、光互连等应用十分重要。一种实现定向耦合的方法是利用少数几个人工微结构的散射和干涉，例如把两个可等效为偶极子的纳米结构放置在波导上方，通过改变结构相对间距以及尺寸可以调整偶极子间的相位差，从而实现高方向性入射耦合[49,71-72]。2012 年，Arango 等[73]将一维波导与金纳米天线阵列相集成，通过偶极子天线间的相互耦合以及波导对天线间耦合作用的增强，实现了自由空间光定向耦合入波导，如图 2(a)所示。此外，纳米天线的共振和散射属性可以被设计成偏振或波长选择的，从而实现偏振、波长的多路复用[52]。Guo 等[53]通过将两个对入射偏振响应不同的纳米天线组合在一起，实现了可用于高速光通信的片上集成偏振解复用器。该结构可以将不同偏振的自由空间光转变为沿相反方向传输的不同波导模式，从而实现了超紧凑的光路由。另一种实现定向耦合的方法是利用相位梯度超构表面所提供的单向相位梯度。2014 年，Pors 等[74]基于间隙表面等离子激元

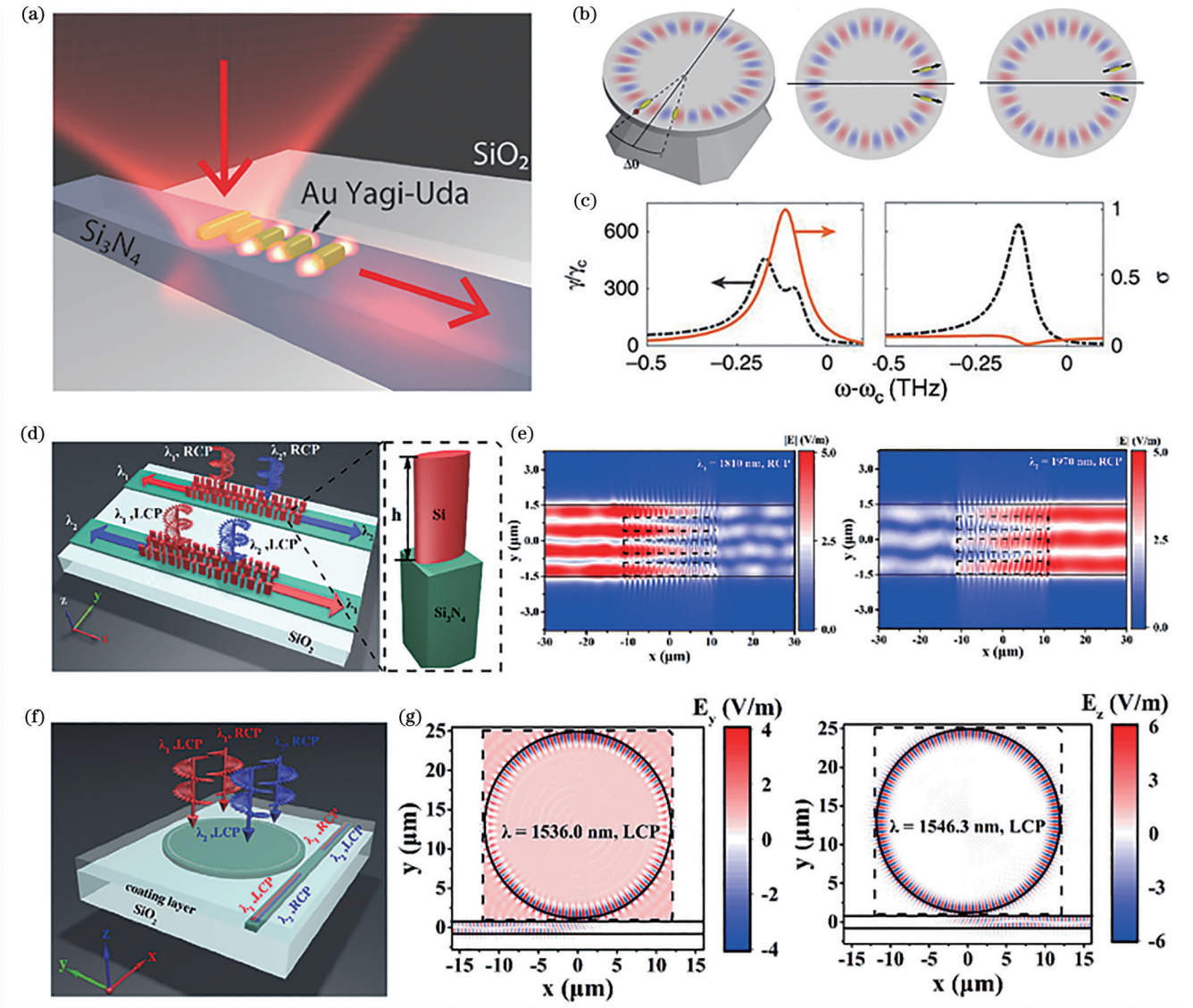

图 2　基于片上集成人工微结构的入射耦合调控。(a)氮化硅波导集成金纳米天线阵列示意图[73];(b)微盘上集成天线二聚体结构示意图[79];(c)局域态密度增强倍数(虚线)和定向性(实线)随两个天线的频率移动 $\omega-\omega_c$ 的变化[79];(d)基于片上集成几何超构表面的自旋选择波长解多路复用示意图[83];(e)不同波长的右旋圆偏振光入射时,波导中心 x-y 平面上的电场振幅分布[83];(f)基于超构表面集成微腔的多带片上 PSHE 示意图[85];(g)不同波长的左旋圆偏光入射时,波导和微腔横截面上的电场分量分布[85]

Fig. 2　Input-coupling manipulation based on on-chip integrated artificial microstructure. (a) Schematic of Si_3N_4 waveguide with an array of gold nano-antennas[73]; (b) schematic of an integrated antenna-dimer on a micro-disk[79]; (c) variation of local density of states enhancement factor (dashed line) and directionality (solid line) as a function of frequency shift $\omega-\omega_c$ between two antennas[79]; (d) schematic of spin-selective and wavelength-selective demultiplexing based on on-chip integrated geometric phase metasurface[83]; (e) electric field amplitude distribution in x-y plane bisecting waveguide for right-handed circularly polarized incident light with different wavelengths[83]; (f) schematic of on-chip multi-band PSHE based on metasurface integrated microcavity[85]; (g) distribution of electric field components on cross-section of waveguide and microcavity for left-handed circularly polarized incident light with different wavelengths[85]

(GSP)共振阵列,提出了一种可将两束正交线偏振光路由到不同方向的超耦合器。2016 年,该团队进一步在波导上设计了三个基于 GSP 的超构表面,用于单向激发沿着六个不同方向传播的波导模式,这些方向对应于斯托克斯参数定义的三种正交偏振基矢 $[(\hat{x},\hat{y})、(\hat{a},\hat{b})、(\hat{r},\hat{l})]$[75],从而实现了片上的偏振测量计。回音壁模式(WGM)微腔可以把光场限制在一个很小的体积内,具有高的品质因子 Q、小的模式体积 V 等优势,在非线性光学、量子光学、传感等领域都有重要应用。但由于光学微腔的高对称性,很难将自由空间光直接耦合到微腔中。将人工微结构集成在片上光学微腔上[76-78],不仅可以将自由空间光直接耦合入微

腔中，而且可以增加调控微腔模式的手段，实现更丰富的功能。例如，Cognée等[79]在WGM微盘腔上集成了一对相同尺寸的铝纳米天线，实现了荧光的定向注入。该结构示意图如图2(b)所示，微腔上方的二聚体纳米天线可以看作是一个最小的相控阵列，它们可以通过微腔模式实现协同共振。通过改变二聚体金属粒子间的夹角$\Delta\theta$，可以调控两个天线间的“偶极子-偶极子”相互作用，从而实现定向耦合。图2(c)展示了两种不同θ下的局域态密度增强倍数(γ/γ_c)(虚线)和定向性σ(实线)随着两个天线的频率移动$\omega-\omega_c$的变化，$\Delta\theta=0.81$时，σ为1，γ/γ_c超过300(左图)，$\Delta\theta=1.25$时，σ几乎为0，γ/γ_c大于600(右图)，很好地证明了金属二聚体增强辐射和定向性的能力。

尽管片上集成等离子体天线可实现超紧凑的定向耦合器，但其制造过程一般与互补型金属氧化物半导体(CMOS)工艺不兼容，而且金属微结构的散射损耗和其固有的欧姆损耗[80]使其难以实现高效率的入射耦合。利用硅和二氧化钛等电介质纳米结构[81]可以很好地解决以上问题。2018年，Guo等[82]将金属和电介质超构表面分别与绝缘层上硅(SOI)波导集成在一起，实现了入射圆偏振光的定向耦合。其基本原理是基于超构表面所提供的Pancharatnam-Berry(PB)相位(又称为几何相位)梯度。根据PB相位理论[24]，当一束圆偏振光正入射在一个几何尺寸固定、转角分布为$\theta(x,y)$的微结构阵列上时，产生的正交圆偏光的相位分布为$\varphi(x,y)=2\sigma\theta(x,y)$，$\sigma=\pm1$分别对应于左旋/右旋圆偏振入射光。当各向异性纳米结构转角从0旋转到π时，对于相反旋性的圆偏振出射光，相位可以从0变化到2π。将固定转角梯度的结构依次排列在波导上方，便能为不同圆偏振入射光提供单向的相位梯度，从而使它们沿相反方向单向耦合到波导里。理论计算表明，使用电介质人工微结构可以大幅提升入射光的耦合效率[82]。2019年，Zhang等[83]提出了一种在氮化硅波导顶部集成几何相位型硅(Si)超构表面的设计，实现了自旋选择定向耦合和波长解复用，如图2(d)所示。基于波导内部电磁场的固有手性分布[84]，如果将天线阵列置于波导手性点上，则入射圆偏振光会单向耦合到波导中，这种效应被称为“自旋-动量锁定效应”，利用该原理并结合相位匹配条件便可实现在右旋圆偏振光入射情况下，两个不同波长的入射光激发的不同波导模式向相反方向传播，如图2(e)所示。2021年，该团队又提出了将超构表面与微腔集成在一起来实现多带片上光子自旋霍尔效应(PSHE)和选择性激发WGMs的方法[85]。自旋角动量相反的自由空间圆偏振光可以在固定波长下激发传播方向相反的WGMs，如图2(f)所示。图2(g)显示了激发的波导和微腔模式的电场分量，在1536.0 nm处，电场以E_x和E_y为主，激发的微腔模式为顺时针传播的横电(TE)模式，耦合到波导中后向左传播。在1546.3 nm处激发的微腔模式由电场E_z主导，激发的微腔模式为逆时针传播的横磁(TM)模式，耦合到波导中后向右传播。与文献[83]实现的宽带片上PSHE相比，将超构表面与微腔集成，不仅可以实现自由空间光与微腔之间的直接耦合，而且可实现窄带的多波段片上PSHE。

以上工作只实现了线偏振光或圆偏振光的入射耦合，若要实现任意入射偏振态的定向耦合，可同时利用传播相位和几何相位[86]。2019年，Meng等[87]提出了利用氮化硅波导集成超构表面实现任意偏振入射光定向耦合以及对耦合模式的相位和偏振进行调控的方法。该方法将琼斯矩阵模型[88]引入到片上系统中，结合广义斯涅尔定律[23]，可以得到入射光和目标波导模式间的相位差，由片上微结构的传播相位和几何相位来补偿。如果入射光是一对正交偏振光，则可以得到两个独立的相位分布，实现片上偏振分离以及波导模式TE_{00}和TM_{00}的定向耦合。随后该团队进一步考虑了相位匹配条件，大大提高了耦合效率，并且通过调整天线阵列的相对位置，优化天线散射的近场和目标波导模式之间的场重叠，实现了高纯度的高阶波导模式(如TE_{01}、TE_{10}、TM_{11}和TM_{20})的选择性激发[54]。虽然目前的超耦合器已经实现了对不同偏振和波长的入射光的定向耦合，但它们对入射光的不同相位分布还无法做到有效区分，怎样实现对入射光的入射角度或轨道角动量(拓扑荷数)的精确识别和定向耦合是该领域未来研究的一大难点。

3 基于片上集成人工微结构的导波模式面内调控

利用人工微结构除了可以将自由空间光耦合到波导内，还可以实现导波模式的面内调控，实现模式转换、片上光场聚焦等功能。与传统的模式转换器[89]相比，引入人工微结构可以实现紧凑、宽带、高效率的面内模式转换。如图3(a)所示，模式转换可以通过利用波导表面浅刻蚀的纳米结构所带来的折射率周期性扰动来实现[90]。在矩形硅波导顶部蚀刻亚波长微结构，可产生沿传播方向的周期性扰动$\Delta\varepsilon(x,y,z)$和垂直于传播方向的渐变折射率分布，如图3(b)所示。利用有效介质理论[91-92]，周期性扰动提供不同模式之间的相位匹配，渐变折射率分布提供模式之间的交叠，用来增强耦合强度，最终在1 μm×220 nm尺寸的硅波导中成功将TE_0模式转换为TE_1模式。模式转换是模式复用系统的基本要求，多模转换的关键是对多模实现同样高的转换效率，由于不同模态对之间的相位匹配条件存在显著差异，仅使用基于周期扰动的相位匹配技术难以实现。Cheng等[93]在硅平板波导上浅刻蚀二维分布的六边形槽，通过引入沿波导横向的周期性扰动和

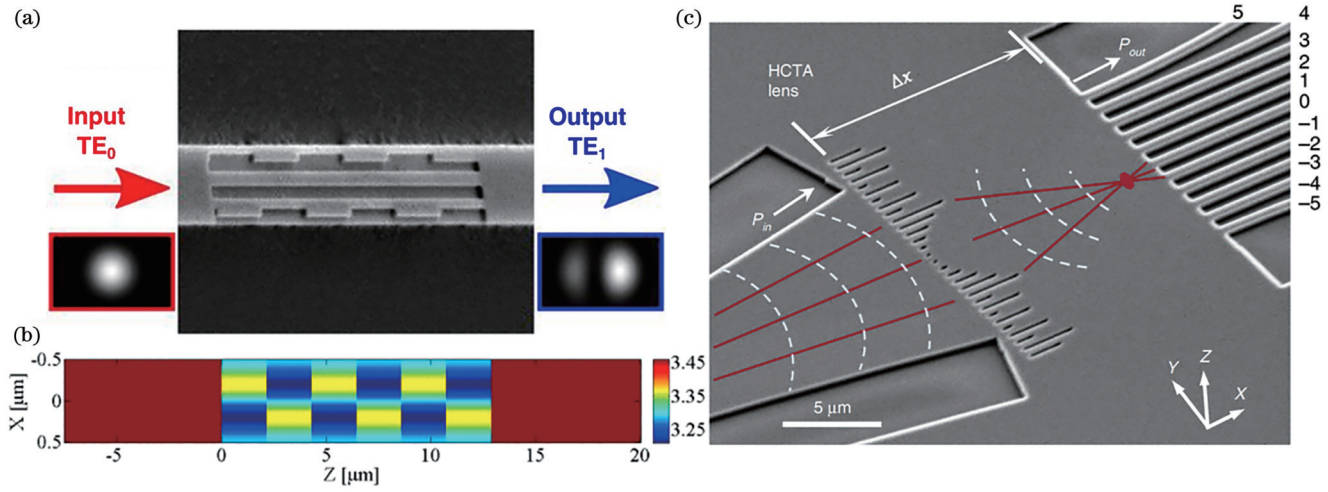

图 3　基于片上集成刻蚀微结构的波导模式面内调控。(a)基于浅刻蚀超构表面的波导模式转换器示意图[90];(b)模式转换所需的超构表面折射率分布[90];(c)超紧凑片上低损耗超构透镜示意图。在输出平面上放置了 11 个单模波导用于得到光强分布[56]

Fig. 3　In-plane manipulation of waveguide modes based on on-chip integrated etching microstructures. (a) Schematic of a waveguide mode converter based on shallow-etched metasurfaces[90]; (b) refractive index distribution of metasurface required for mode conversion[90]; (c) schematic of ultra-compact on-chip low-loss metalens. Eleven single-mode waveguides are placed on output plane to obtain light intensity distribution[56]

纵向的非周期性扰动，同时实现了三种低损耗和低串扰的不同模式转换过程，为并行光学信息处理系统的设计和实现提供了思路。

上述工作都需要在制造过程中至少进行两步光刻，并且是针对固定宽度波导内的模式转换。和浅刻蚀方式相比，全刻蚀可以简化制作过程、节约成本。Yao 等[94]通过在 SOI 波导上全刻蚀 Si 纳米孔结构实现了高效波导模式转换。当入射波长为 1.55 μm 时，仅使用约 2.42 μm 的转换长度，便可在实验上实现效率高达 83.1% 的从 TE_{00} 到 TE_{10} 的模式转换。通过改变槽结构的尺寸和排列方式可以调控结构的传输矩阵，实现多种模式转换[95]。2019 年，Wang 等[56]通过在 SOI 波导上全刻蚀一个一维高对比度传输阵列(HCTA)透镜实现了高效率的导波面内聚焦，如图 3(c)所示。该结构可以将直径为 11 μm 的导波快速收缩为半峰全宽仅为 0.75 μm 的焦点，并且可以在带宽 200 nm 内保持聚焦效率在 74% 以上，显著缩短了模式尺寸转换所需的锥形区长度。该团队在一维 HCTA 设计的基础上，通过级联三层 HCTA 结构，进一步实现了可用于傅里叶变换和微分操作的光学计算系统，为大规模、超紧凑硅光子计算芯片的设计提供了新的方案。

此外，也可以通过直接在波导上方集成人工微结构实现波导内部模式转换和波前调制[96]。2017 年，Li 等[97]在波导上集成等离子体/电介质纳米天线组成的梯度超构表面，在红外波段通过微结构提供单向相位梯度实现了波导内模式转换和模式的非对称传输。2019 年，Wang 等[98]利用类似的原理扩展到 THz 波段实现了带宽高达 100 GHz 的片内非对称传输。2020 年，Fan 等[99]将基于金等离子体超构表面的轴透镜集成在 Si 波导上，实现了无衍射的贝塞尔光束的近场成像，如图 4(a)所示。通过等离子体纳米天线的谐振可改变硅波导局部有效折射率($\Delta n \approx 0.22$)，一束 10 μm 宽的高斯光经过轴透镜后被分为两束斜折射(折射角大约为 3°)光束，通过干涉效应形成贝塞尔光束，如图 4(b)所示。图 4(c)展示的光束强度分布与分别用高斯和贝塞尔-高斯拟合的输入和输出光束的强度分布一致，证实了片上集成轴透镜的有效性。2022 年，Deng 等[100]利用片上集成 C 型金超构表面，在 1550 nm 通信波段内实现了高阶 TM 模式到 TE 模式的转换以及正交偏振模式的波前调控。C 形纳米天线可同时支持垂直于对称轴的平面内电偶极子模式和沿 z 方向的平面外磁模式[101-102]。因此，当 TM 模式入射到超构表面处时，其倏逝波分量 E_x 可诱导产生面内的电偶极矩和面外的磁偶极矩，从而产生相位可随转角变化的 E_y 分量，进而实现正交偏振模式转换与导波的面内聚焦[100]。

片上集成人工微结构还可以与铌酸锂(LN)等材料结合在一起，实现导波模式的动态调控。LN 拥有较高的折射率和较大的电光系数(波长为 630 nm 时，$r_{33} = 30.8 \times 10^{-12}$ m/V)，且响应速度较快[103]，被广泛应用于高速电光调制器件。近些年研究人员提出了一种铌酸锂单晶薄膜——绝缘体上的铌酸锂(LNOI)[104]，通过 LN 和衬底之间的高折射率对比度，可以有效地将光限制在亚波长尺度上，促进了紧凑型片上集成电光调制器件的发展。薄膜 LN 上的马赫-曾德尔干涉仪(MZI)或环辅助 MZI 调制器具有带宽大、驱动电压低的优点[105-106]，然而，它们往往需要结合长

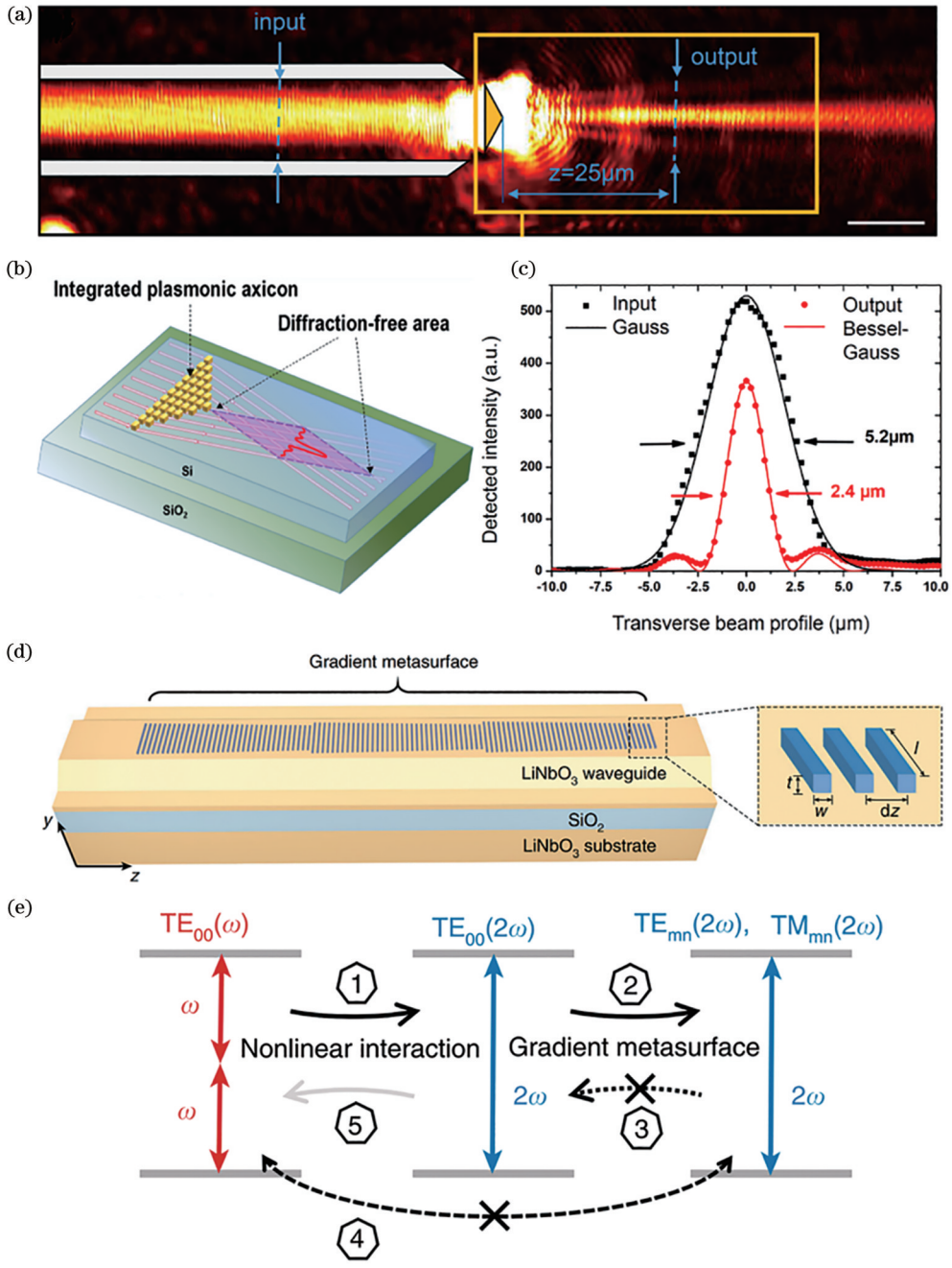

图 4　基于片上集成超构表面的波导模式面内调控。(a)基于末端耦合的扫描近场光学显微镜测量的电场强度分布[99];(b)集成在SOI波导上的二维等离子体纳米谐振器阵列形成的贝塞尔光束发生器示意图[99];(c)分别用高斯和贝塞尔-高斯函数拟合的输入和输出光束的横截面[99];(d)片上集成非线性光子器件结构示意图[60];(e)二次谐波产生过程概念图[60]

Fig. 4　In-plane manipulation of waveguide modes based on on-chip integrated metasurfaces. (a) Electric field intensity distribution measured by scanning near-field optical microscopy based on end-coupling[99]; (b) schematic of a Bessel beam generator formed by a two-dimensional array of plasmonic nano-resonators integrated on SOI waveguide[99]; (c) transverse profiles of input and output beams fitted with Gaussian and Bessel-Gaussian functions, respectively[99]; (d) schematic of an on-chip integrated nonlinear photonics device structure[60]; (e) conceptual diagram of SHG process[60]

为 3～20 mm 的移相器，导致较大的设备面积占用。2020 年，Li 等[107]利用挖槽电介质波导实现了基于光子晶体纳米梁谐振器的高速 LN 电光调制器。该器件表现出高达 1.98 GHz·V^{-1} 的调谐效率，调制带宽为 17.5 GHz，电光模式体积只有 0.58 μm^3。最近，Zhang 等[61]在薄膜铌酸锂集成平台上实现了一维晶格中的拓扑界面态。通过在氮化硅波导上方设计周期性排列的矩形空气孔结构，可以调控波导的有效折射率。由于界面态的强光学约束和电光响应的峰值增强，一个尺寸仅为 1.6 μm×140 μm 的拓扑调制器可实现 104 GHz 的大调制带宽，有望为高速率、低功耗和低成本的 LN 光子集成光路提供新的解决方案。

另外，LN还具有较大的二阶非线性极化率[103]，是研究非线性光学过程的理想材料。非线性频率转换过程中的一个关键因素是相位匹配，它要求该过程中所涉及的光子动量守恒。传统非线性相位匹配通常是使用具有双折射性质或周期极化的非线性晶体实现的，需要精心的色散设计，并且通常是窄带的[108-109]。2017年，Yu等[60]提出了一种基于梯度超构表面结构和非线性LN波导集成的无相位匹配非线性二次谐波产生(SHG)过程，如图4(d)所示。基本原理如图4(e)所示：首先，光功率在LN波导中从泵浦$TE_{00}(\omega)$模式耦合到二倍频的基模$TE_{00}(2\omega)$(图中的箭头1)；然后在梯度超构表面的帮助下，$TE_{00}(2\omega)$耦合到二倍频下的高阶模式$TE_{mn}(2\omega)$和$TM_{mn}(2\omega)$(箭头2)，梯度超构表面提供的单向波矢确保了高阶模耦合到倍频基模的效率极低(箭头3)；由于在波导截面上高阶模和基频基模之间的空间重叠很小，从高阶模到基频基模的光功率耦合效率也非常低(箭头4)。这样，就实现了泵浦光到二倍频信号的单向光功率传输，且是宽带的(波长在1580～1650 nm范围内)。但是由于高阶模达到波导截止条件后会被耦合出来，所以SHG转化效率只能在有限作用距离范围内随着纳米天线阵列的增加不断增大[60]。人工微结构不仅可以用来提高SHG效率，还可对产生的非线性光场进行波前调控。2020年，Fang等[110]通过在LNOI平板波导上引入亚波长光栅超构表面，利用超构表面提供的倒格矢相位匹配，可以将空间传输的基频光有效地转化为二倍频。同时超构表面还将振幅和相位信息编码到光栅结构中，从而可以对产生的倍频光进行波前调控，实现波导内双焦点聚焦和Airy光束。将人工微结构与薄膜LNOI平台相结合可以为片上光场的动态调控或片上集成非线性光学元件的研发提供更多可能性。然而，目前LN样品的制备技术仍面临一些不足，比如现有的制备方法难以实现侧壁接近垂直的LN结构和一些尺寸较小、形状较复杂的LN纳米孔或纳米柱结构。此外，将其他电介质或金属材料加工到LN波导或微腔上需要使用较复杂的多次刻蚀工艺，不利于相关器件的大面积制备。但是，考虑到LN材料出色的光学特性及其广泛的应用前景，加之薄膜LN制备技术的日益精进，我们有理由相信，基于这一平台的片上集成人工微结构将在未来的光子集成芯片领域发挥举足轻重的作用。

4 基于导波驱动超构表面的远场辐射调控

将片上集成光学元件中的导波耦合到自由空间中是实现光学探测与分析、图像展示、光学信息传输等功能的关键步骤。在导波和自由空间光远场模式之间转换时，有一个可以灵活操控光的界面非常重要。然而，表面光栅[111]和边缘耦合器[112]等传统的界面功能有限，很难实现2π相位的连续调控，而且损耗大，难以实现对光的完全控制。近几年，研究者们通过将人工微结构和波导/微腔相结合，利用导波模式来驱动超构表面，直接把导波耦合到自由空间中，并将其塑造成所需的光场，实现了多种新颖的光学应用。同时超构原子的亚波长间距可以避免衍射损失，允许更紧凑的片上集成，为超紧凑光子集成光路的设计提供了新的思路和更多的调控自由度。

4.1 导波驱动超构表面对远场辐射的单维调控

导波驱动超构表面可以将片上的导波模式通过人工微结构转化为远场辐射，并对它们的振幅、相位、偏振等维度进行调控。与自由空间超构表面不同，导波驱动超构表面提取的波的总相位主要由两部分组成[66]，如图5(a)所示：1)导波沿传播方向的相位积累βx(假设导波在矩形波导中沿着x方向传播，β是导波模式的传播常数)；2)每个超构原子在坐标x处引起的突变的且随空间位置变化的相移$\Delta\phi(x)$。所以提取的辐射波沿x方向的相位分布可以表示为：$\varphi(x)=\beta x+\Delta\varphi(x)$。为了实现对波前的完全控制，需要超构原子实现0～2π的相位覆盖。2020年，Guo等[66]在Si波导上通过构建金属-电介质-金属(MIM)型纳米结构，利用波导中的传播相位和MIM型纳米结构的谐振相位叠加实现了辐射场2π范围的相位调控。该超构表面由一组相位梯度为$\partial\Delta\varphi/\partial x$的超构原子组成，从正向传播的导波中提取的光的横向波矢量$k_x=\beta+\partial\Delta\varphi/\partial x$，它以角度$\theta=\sin^{-1}(k_x/k_0)$辐射到自由空间，进而实现了面外光束偏转，如图5(b)所示。反向传播的导波中提取的光的横向波矢量为$k_x=-\beta+\partial\Delta\varphi/\partial x$，超过了自由空间中的最大可支持波数，因此，它被束缚在超构表面上，最终由于材料的欧姆损耗而消失。该工作为导波驱动超构表面远场辐射调控奠定了一定理论基础。2022年，Ding等[113]在平板波导上放置二维分布的MIM超构表面，实现了片外二维聚焦和全息，该工作可以用于许多其他需要二维光场调控的光学应用，如固态激光雷达[114-115]、增强现实和虚拟现实设备[116-117]等。值得注意的是，文献[66]和文献[113]都是利用MIM结构辐射导波，所以导波传输过程中损耗较大，而且采用的是共振相位，实现2π相位覆盖往往需要复杂的参数优化过程，同时很难保持振幅稳定。2021年，Fang等[118]引入Si几何超构表面作为导波和自由空间辐射光的界面，实验上实现了片外聚焦、多通道涡旋光束和全息成像功能，如图5(c)所示。因其使用的单个超构原子的辐射效率较低，可以在铌酸锂平板波导上级联多个超构表面阵列产生不同拓扑荷数的聚焦轨道角动量(OAM)光束。与通过改变结构尺寸实现的谐振相位相比，几何相位依靠人工微结构的转角，具有设计简单、损耗小、对结构尺寸鲁棒性好等优势。

以上工作都局限于对片上单个方向入射的研究，

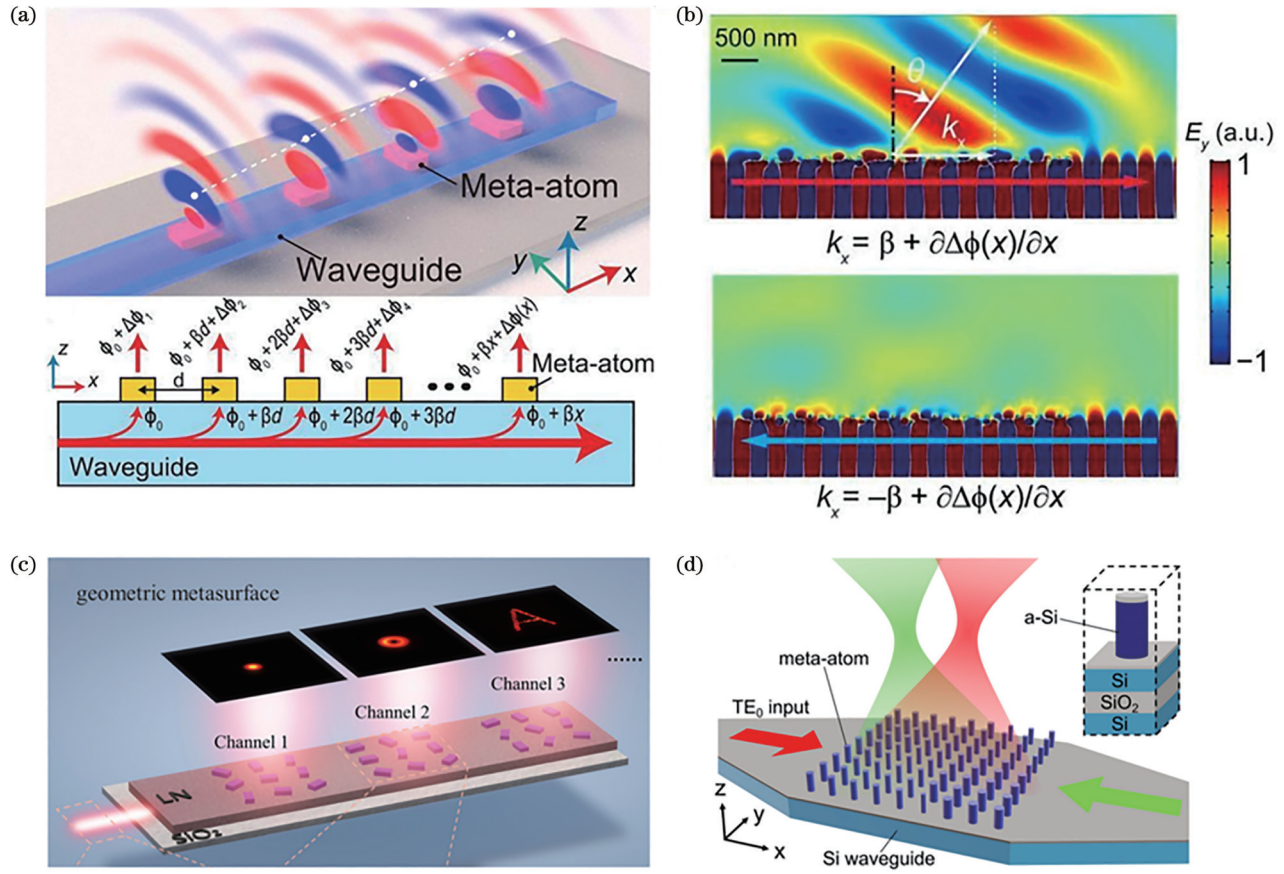

图 5　导波驱动超构表面远场辐射的一维光场调控。(a)导波驱动超构表面远场辐射调控示意图[66];(b)正向(上)和反向(下)传播的导波驱动的相位梯度超构表面提取光的电场分布[66];(c)针对 LNOI 光子光路的片上集成多功能超构表面示意图[118];(d)硅波导上集成超构表面实现可切换光束聚焦示意图[119]

Fig. 5　One-dimensional optical field manipulation of far-field radiation from guided wave-driven metasurfaces. (a) Schematic of guided wave-driven metasurface for far-field radiation manipulation[66]; (b) electric field distribution of extracted light from phase-gradient metasurface driven by forward propagating (above) and backward propagating (below) guided waves[66]; (c) schematic of on-chip integrated multifunctional metasurface for lithium niobate on insulator (LNOI) photonic circuit[118]; (d) schematic of silicon waveguide integrated metasurface for switchable beam focusing[119]

可承载的信息容量有限。Hsieh 等[119]通过双端口分别入射,实现了片外可切换双焦点聚焦,如图 5(d)所示。当导波从不同方向入射时,所积累的传播相位是符号相反的。超构表面所提供的共振相位会在聚焦相位的基础上给辐射光附加单向的横向波矢,此横向波矢会与其中一个端口入射的导波的传播波矢同向,而与另一个端口的波矢反向,从而使辐射光聚焦到不同的横向位置。2021 年,Ha 等[63]在 Si 波导上浅刻蚀矩形纳米孔,通过粒子群优化算法结合迂回相位在理论上实现了 $\pm x/y$ 方向解耦的四路复用全息。但是这种设计主要依赖于算法优化,设计的灵活性不高。最近,Yang 等[120]提出一种迂回相位和几何相位复合的方法,通过几何相位打破 $\pm x(y)$ 方向的迂回相位简并性,实现了基于片上超构表面的四重解耦多路复用全息,为片上集成高容量光通信提供了一种新方式。

4.2　基于单端口入射的远场辐射多维调控

为了进一步提高导波驱动超构表面的远场辐射调控能力,研究者对辐射场的相位、振幅、偏振、波长等多个自由度的联合调控展开了研究,通过对辐射场的多维调控以及多端口入射,进一步丰富了导波驱动超构表面的远场辐射功能。2021 年,Cognée 等[121]结合等离子体纳米天线和微盘腔,通过对辐射场相位和偏振的二维调控,实现了单偏振态纯 OAM 光束的产生,如图 6(a)所示。具体来说,每个天线等价于一个右旋和一个左旋圆偏振偶极子辐射源的叠加,可以同时散射出不同拓扑荷的左右旋圆偏光。产生的拓扑荷数 l 满足选择定则 $l = m - N \pm 1$,其中,m 是 WGM 腔的方位角模数,N 是天线数量。通过合理设计二聚体等离子天线间的夹角 $\Delta\varphi$,利用 $\Delta\varphi = -\pi/2N$ 的“V 型”结构,以及 $\Delta\varphi = +\pi/2N$ 的“Λ 型”结构,分别可以抵消右旋和左旋圆偏振光,只让左旋和右旋圆偏振光辐射到远场,如图 6(b)所示。最近,Zhang 等[122]提出了一种利用导波驱动的几何超构表面同时实现片上远场辐射偏振和相位调控的新方法,如图 6(c)

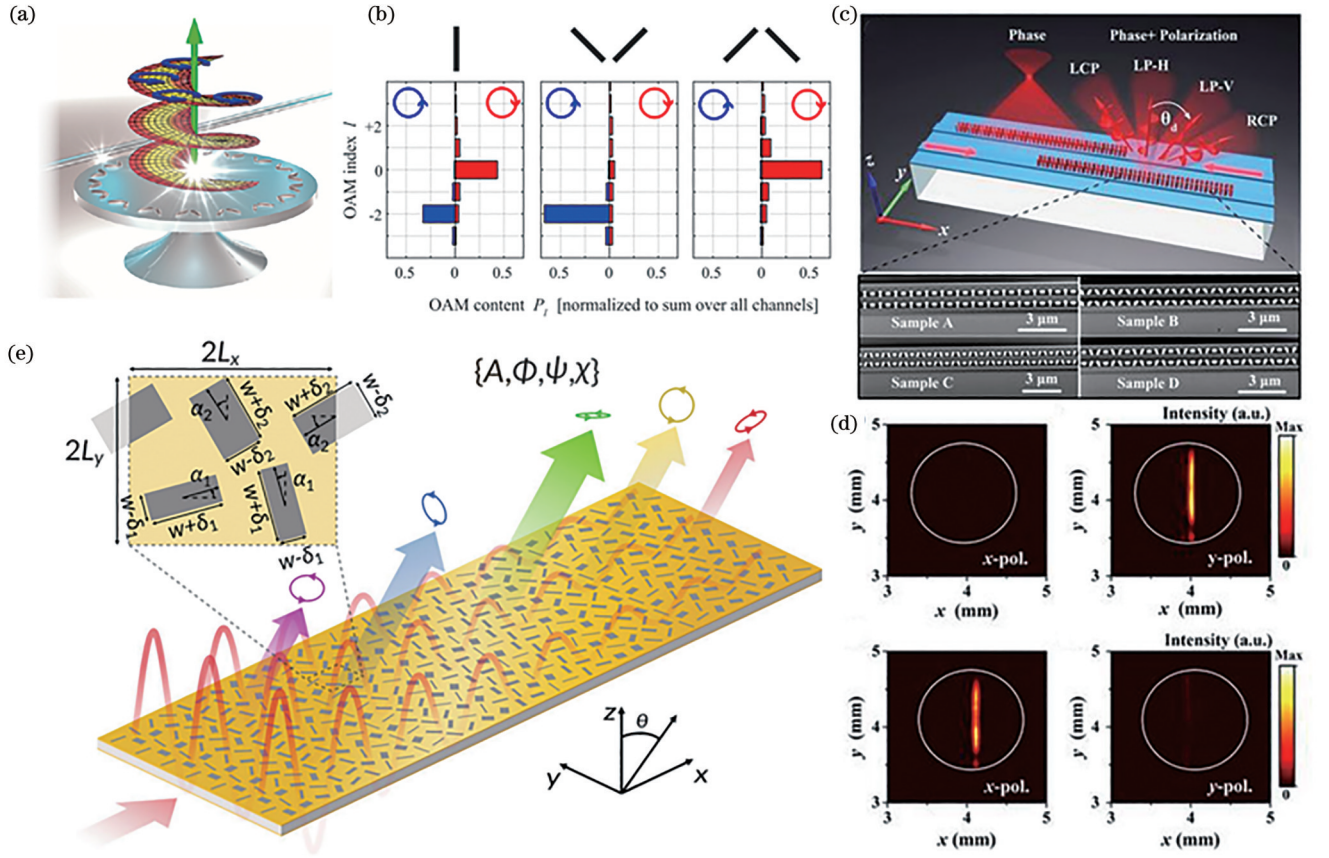

图 6　基于单端口入射的导波驱动超构表面远场辐射多维调控。(a)用等离子体天线链装饰的微盘谐振器示意图[121];(b)径向型、V型和Λ型结构的模态分解直方图。在每幅小图中，$m-N=-1$[121];(c)导波驱动几何超构表面实现远场相位和偏振调控示意图。插图为产生不同偏振态的样品的扫描式电子显微镜图像[122];(d)实验得到的从样品A和样品B辐射的x偏振光和y偏振光的傅里叶平面图像[122];(e)支持q-BICs的漏波超构表面示意图[124]

Fig. 6　Multi-dimensional manipulation of far-field radiation using guided wave-driven metasurfaces with single-port input. (a) Schematic of microdisk resonator dressed by a chain of plasmonic antenna[121]; (b) mode decomposition histogram for radial, V-shaped, and Λ-shaped structures. In each graph, $m-N=-1$[121]; (c) schematic of guided wave-driven geometric metasurface for far-field phase and polarization control. Insets are scanning electron microscope images of fabricated samples that can generate different polarization states[122]; (d) Fourier plane images of x-polarized and y-polarized lights radiated from samples A and B obtained experimentally[122]; (e) schematic of a leaky-wave metasurface supporting q-BICs[124]

所示。该方法利用了椭圆纳米柱超构原子产生的几何相位改变以及脊型波导内部场强横向分布不均匀的特点，通过超构原子的旋转角度来调控辐射光的相位，通过超构原子相对于波导中心的横向位移来调控辐射光的振幅，通过超构原子之间的远场干涉来调控辐射光的偏振，进一步可产生辐射角度可调的不同偏振光束。图6(d)是测量得到的从样品A和样品B辐射的x和y偏振光的傅里叶平面图像。可以看到样品A辐射y偏振光，样品B则辐射x偏振光，与设计一致。Huang等[123]引入了漏波超构表面，基于支持准连续体中束缚态(q-BIC)的对称性破缺光子晶体板，实现了近红外波段下片外辐射场振幅、相位、偏振态的全参量调控，为片上超构表面光场调控提供了新思路。同年，Xu等[124]利用类似的方法，研究了在微米/毫米波频率下工作的片上漏波超构表面，这些天线基于q-BIC原理设计，通过合理设计结构对称性，可以把波导模式完全泄漏出来。进一步通过优化超胞的转角、结构尺寸以及结构间距等参数可以实现对漏波的全参量(振幅A、相位φ、椭偏度ψ、方位角χ)调控，如图6(e)所示。该研究在实验上实现了单输入多输出和多输入多输出的波束聚焦以及波束偏振态调制，为高性能、超紧凑的无线收发器设计提供了新的方案。

4.3　基于多端口入射的远场辐射多维调控

片上集成光路为多端口同时入射提供了便利，简化了多光束干涉相关研究的实验光路，并且为多功能片上光学元件提供了更多设计自由度。将多端口入射与片上集成人工微结构结合在一起，可进一步扩大信道容量或增加功能的多样性[125]。在此基础上结合辐射场多维调控以及引入动态调控可以进一步促进高集成度、低损耗、多功能以及灵活可调片上集成器件的发展。2022年，Shi等[126]通过片上人工微结构的迂回相

位和PB相位联合调控，结合双波导通道和自由空间通道，实现了对辐射场相位和波长的同时调控，实验上观察到了三通道复用彩色全息。随后，他们构造了双超构原子，利用双原子间位移D及干涉作用，实现了对近场光散射强度的有效调控[127]。如图7(b)所示，光提取效率随着位移D的变化而周期性地波动。同时，结合超构原子两个入射方向相互独立的迂回相位调制，实现了对导波辐射场振幅、相位和波长三个维度的调控，最终在实验上实现了与双通道独立编码全息投影同步的屏显技术，如图7(a)所示。同年，Ji等[125]提出并演示了一种基于LNOI平台的导波驱动超构表面实现片上产生和调控高阶庞加莱球(HOP)光束的方法，如图7(c)所示。其原理是利用双原子几何超构表面的相位调控，将导波以两个拓扑荷相反的正交圆偏振涡旋光耦合到自由空间中进行线性叠加，生成HOP光束。同时，通过双原子干涉可以消除未调制的辐射，提高辐射光的信噪比。值得关注的是，该研究是通过光学元件调控入射到双端口的振幅和相位差来展示偏振态演化过程的，为完全集成的片上光场动态调控奠定了基础。为了进一步提升多路复用通道数量，该团队又提出了一种片上集成非均匀排列几何超构表面平台，基于x、y方向迂回相位和几何相位3个自由度，实现了独立的3通道导波辐射波前调控，通过对辐射场相位和波长的调控，实现了偏振解复用、波长解复用以及彩色全息[128]。多端口入射结合多维光场调控极大地拓展了集成光学器件的功能，再结合动态调控[62,129-130]，可以进一步促进该领域的发展。

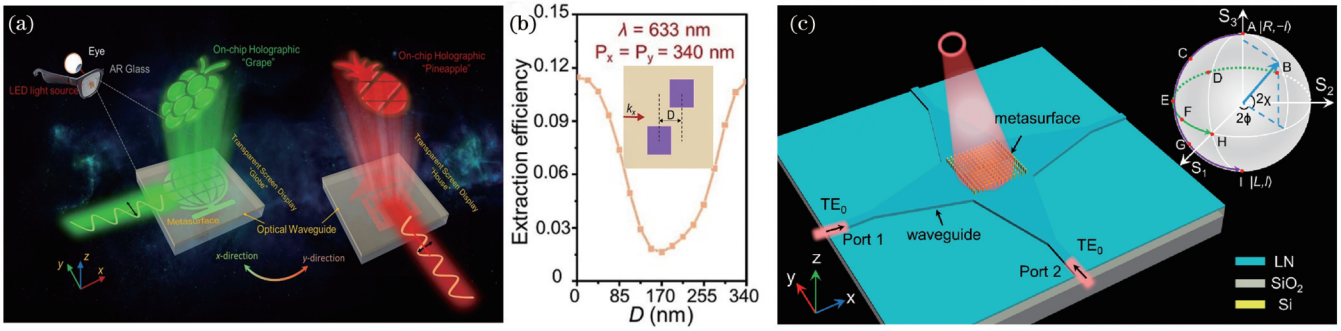

图7　基于多端口入射的导波驱动超构表面远场辐射多维调控。(a)片上集成超构表面实现半透明屏显与同步全息投影[127]；(b)在633 nm的波长下，超构原子外提取效率随原子间距D的变化曲线[127]；(c)在LNOI平台上利用超构表面实现HOP光束示意图。插图为HOP示意图[125]

Fig. 7　Multi-dimensional manipulation of far-field radiation using waveguide-driven metasurfaces with multi-port input. (a) On-chip integrated metasurfaces for semi-transparent screen display in sync with holographic projection[127]; (b) external extraction efficiency of meta-diatoms as a function of displacement D between two meta-atoms at a wavelength of 633 nm[127]; (c) schematic of higher-order Poincaré sphere (HOP) beams achieved by metasurfaces integrated on LNOI platform. Inset is illustration of HOP[125]

值得注意的是，尽管导波驱动超构表面近年来取得了令人振奋的进展，然而要将它们转化为实际商业应用，仍然面临着诸多挑战。其中一项关键挑战来自于波导下方的基底。由于基底材料的折射率一般大于空气折射率，当人工微结构的间距较大时，基底一侧更容易发生衍射。为了防止此类衍射的发生，需要采用更小尺寸的人工微结构和更小的结构间距。然而，这样做却会给导波驱动超构表面的设计带来很大限制。另外，由于波导的折射率与基底材料的折射率更接近，从人工微结构散射出的光更容易进入基底。若无特殊的设计和优化，泄漏到基底里的光能量往往会大于直接辐射到空气中的光能量，从而降低器件的工作效率。为解决以上问题，可以使用零折射率材料[6-7]或多层反射结构做基底，也可以通过多种共振模式之间的干涉或特殊结构设计实现单向辐射，从而减少或消除光场向基底的泄漏。

5　总结与展望

本文系统介绍和讨论了片上集成人工微结构在光场调控方面的研究现状与最新进展，从自由空间光场的入射耦合、片上光场不同模式间的相互转化，以及复杂辐射远场的生成等方面讨论了利用片上集成人工微结构调控光场的基本原理、新奇功能与各种应用。尽管部分片上集成人工微结构仍面临效率较低、加工难度较大、实现功能较单一等挑战，但随着新的设计方案与制备工艺的不断提出，这些挑战有望在不远的将来得到突破和解决。基于目前该领域的发展趋势与所面临的问题，本文对未来一些比较有前景的研究方向做初步的展望。

1) 片上级联超构表面。目前大部分片上集成人工微结构实现的功能都比较单一，利用单个超构表面结构很难实现对光场的多步操纵。将多个不同功能的超构表面在光芯片上通过光波导或微腔级联在一起，

相互协作，可实现单个超构表面无法实现的多功能或多路复用器件[118]。在波导上级联多个光学超构表面不仅可以使片上光学元件更加集成化，而且可以为研究更复杂的光学计算过程提供更多可能[56]。

2）基于新奇物理效应的片上集成人工微结构。连续体中束缚态（BIC）[131-133]、宇称-时间（PT）对称[134-136]和奇异点（EP）[137]等新奇物理效应可以为片上集成人工微结构提供更丰富的物理过程，为减少损耗、单向辐射[138]等关键科学问题提供新的解决方案。具有BIC的片上集成人工微结构可以显著增强光场局域，将基于BIC的片上集成人工微结构与微流通道[139]相集成，有望用于高灵敏度传感。近期，Kühner等[140]将成对非对称纳米棒排列成圆环形，实现了小尺寸、高Q值的径向BIC。该工作有望拓展到片上集成微腔体系中，发挥更大作用。拓扑物理的引入可以为该领域注入新的活力，在光场传输鲁棒性、定向传输等方面提升光子器件的性能。

3）基于新材料和新设计方法的片上集成人工微结构。将片上集成人工微结构与二维材料[141]、薄膜LN[142]等新材料平台相结合，可以将激子、谷自旋、非线性效应等更丰富的现象和效应引入片上集成光路。将增益材料和非增益材料集成在同一个光子芯片上，利用片上集成人工微结构的局域场增强等效应可以为片上微纳激光器[143-144]或非厄密物理[145]的相关研究提供更丰富的调控自由度。并且将片上微纳激光器与人工微结构等片上光场调控元件集成在一起可以更进一步减小器件体积。将二氧化钒[146]、$Ge_2Sb_2Te_5$（GST）[147]等相变材料[14]引入片上集成人工微结构体系中，可以为实现动态调控或可重构的片上集成光学元件提供新的解决方案。未来随着片上集成人工微结构的集成复杂度的增加，传统的优化设计方法在仿真时间、内存需求等方面会遭遇瓶颈。深度学习[148]、拓扑优化[149]等逆向设计[150-156]方法可以部分解决以上问题，为片上集成人工微结构的设计提供强有力的工具。

总的来说，人工微结构为人们实现传统光学元件的片上集成和新颖光学器件的设计提供了丰富的调控自由度和强大的光场调控能力。随着科技的进步，片上集成人工微结构的应用范围会更加广泛，工作波段可从可见光和近红外光向太赫兹波、微波、紫外波段扩展，更加小型化和集成化的片上微纳光子器件也会逐步实现。

参 考 文 献

[1] Cheben P, Halir R, Schmid J H, et al. Subwavelength integrated photonics[J]. Nature, 2018, 560(7720): 565-572.

[2] Zhu D, Shao L B, Yu M J, et al. Integrated photonics on thin-film lithium niobate[J]. Advances in Optics and Photonics, 2021, 13(2): 242-352.

[3] Zhang Y B, Liu H, Cheng H, et al. Multidimensional manipulation of wave fields based on artificial microstructures[J]. Opto-Electronic Advances, 2020, 3(11): 200002.

[4] Ni X J, Wong Z J, Mrejen M, et al. An ultrathin invisibility skin cloak for visible light[J]. Science, 2015, 349(6254): 1310-1314.

[5] Yang Y H, Jing L Q, Zheng B, et al. Full-polarization 3D metasurface cloak with preserved amplitude and phase[J]. Advanced Materials, 2016, 28(32): 6866-6871.

[6] Li Y, Kita S, Muñoz P, et al. On-chip zero-index metamaterials [J]. Nature Photonics, 2015, 9: 738-742.

[7] Tang H N, DeVault C, Camayd-Muñoz S A, et al. Low-loss zero-index materials[J]. Nano Letters, 2021, 21(2): 914-920.

[8] Poddubny A, Iorsh I, Belov P, et al. Hyperbolic metamaterials [J]. Nature Photonics, 2013, 7: 948-957.

[9] Kapitanova P V, Ginzburg P, Rodríguez-Fortuño F J, et al. Photonic spin Hall effect in hyperbolic metamaterials for polarization-controlled routing of subwavelength modes[J]. Nature Communications, 2014, 5: 3226.

[10] He Q, Sun S L, Xiao S Y, et al. High-efficiency metasurfaces: principles, realizations, and applications[J]. Advanced Optical Materials, 2018, 6(19): 1800415.

[11] Ding F, Pors A, Bozhevolnyi S I. Gradient metasurfaces: a review of fundamentals and applications[J]. Reports on Progress in Physics, 2018, 81(2): 026401.

[12] Chen S Q, Li Z, Zhang Y B, et al. Phase manipulation of electromagnetic waves with metasurfaces and its applications in nanophotonics[J]. Advanced Optical Materials, 2018, 6(13): 1800104.

[13] Wen D D, Yue F Y, Liu W W, et al. Geometric metasurfaces for ultrathin optical devices[J]. Advanced Optical Materials, 2018, 6(17): 1800348.

[14] Nemati A, Wang Q, Hong M H, et al. Tunable and reconfigurable metasurfaces and metadevices[J]. Opto-Electronic Advances, 2018, 1(5): 180009.

[15] Chen S Q, Zhang Y B, Li Z, et al. Empowered layer effects and prominent properties in few-layer metasurfaces[J]. Advanced Optical Materials, 2019, 7(14): 1801477.

[16] Cheng H, Liu Z C, Chen S Q, et al. Emergent functionality and controllability in few-layer metasurfaces[J]. Advanced Materials, 2015, 27(36): 5410-5421.

[17] Cheng H, Chen S Q, Yang H F, et al. A polarization insensitive and wide-angle dual-band nearly perfect absorber in the infrared regime[J]. Journal of Optics, 2012, 14(8): 085102.

[18] Li J X, Yu P, Tang C C, et al. Bidirectional perfect absorber using free substrate plasmonic metasurfaces[J]. Advanced Optical Materials, 2017, 5(12): 1700152.

[19] Li Z C, Liu W W, Tang C C, et al. A bilayer plasmonic metasurface for polarization-insensitive bidirectional perfect absorption[J]. Advanced Theory and Simulations, 2020, 3(2): 1900216.

[20] Liu W W, Chen S Q, Li Z C, et al. Realization of broadband cross-polarization conversion in transmission mode in the terahertz region using a single-layer metasurface[J]. Optics Letters, 2015, 40(13): 3185-3188.

[21] Wu P C, Tsai W Y, Chen W T, et al. Versatile polarization generation with an aluminum plasmonic metasurface[J]. Nano Letters, 2017, 17(1): 445-452.

[22] Liu Z C, Li Z C, Liu Z, et al. Single-layer plasmonic metasurface half-wave plates with wavelength-independent polarization conversion angle[J]. ACS Photonics, 2017, 4(8): 2061-2069.

[23] Yu N F, Genevet P, Kats M A, et al. Light propagation with phase discontinuities: generalized laws of reflection and refraction [J]. Science, 2011, 334(6054): 333-337.

[24] Huang L L, Chen X Z, Mühlenbernd H, et al. Dispersionless phase discontinuities for controlling light propagation[J]. Nano Letters, 2012, 12(11): 5750-5755.

[25] Liu Z C, Li Z C, Liu Z, et al. High-performance broadband circularly polarized beam deflector by mirror effect of multinanorod metasurfaces[J]. Advanced Functional Materials,

2015, 25(34): 5428-5434.
[26] Li Z C, Liu W W, Cheng H, et al. Manipulation of the photonic spin Hall effect with high efficiency in gold-nanorod-based metasurfaces[J]. Advanced Optical Materials, 2017, 5(20): 1700413.
[27] Chen X Z, Huang L L, Mühlenbernd H, et al. Dual-polarity plasmonic metalens for visible light[J]. Nature Communications, 2012, 3: 1198.
[28] Khorasaninejad M, Capasso F. Metalenses: versatile multifunctional photonic components[J]. Science, 2017, 358(6367): eaam8100.
[29] Liu W W, Li Z C, Cheng H, et al. Metasurface enabled wide-angle Fourier lens[J]. Advanced Materials, 2018, 30(23): 1706368.
[30] Zuo R Z, Liu W W, Cheng H, et al. Breaking the diffraction limit with radially polarized light based on dielectric metalenses [J]. Advanced Optical Materials, 2018, 6(21): 1800795.
[31] Liu W W, Ma D N, Li Z C, et al. Aberration-corrected three-dimensional positioning with a single-shot metalens array[J]. Optica, 2020, 7(12): 1706-1713.
[32] Wan W W, Gao J, Yang X D. Metasurface holograms for holographic imaging[J]. Advanced Optical Materials, 2017, 5(21): 1700541.
[33] Ma D N, Li Z C, Liu W W, et al. Deep-learning enabled multicolor meta-holography[J]. Advanced Optical Materials, 2022, 10(15): 2102628.
[34] Gao H, Fan X H, Xiong W, et al. Recent advances in optical dynamic meta-holography[J]. Opto-Electronic Advances, 2021, 4(11): 210030.
[35] Yang B, Liu W W, Li Z C, et al. Polarization-sensitive structural colors with hue-and-saturation tuning based on all-dielectric nanopixels[J]. Advanced Optical Materials, 2018, 6(4): 1701009.
[36] Yang B, Cheng H, Chen S Q, et al. Structural colors in metasurfaces: principle, design and applications[J]. Materials Chemistry Frontiers, 2019, 3(5): 750-761.
[37] Yang B, Liu W W, Li Z C, et al. Ultrahighly saturated structural colors enhanced by multipolar-modulated metasurfaces [J]. Nano Letters, 2019, 19(7): 4221-4228.
[38] Yang B, Ma D N, Liu W W, et al. Deep-learning-based colorimetric polarization-angle detection with metasurfaces[J]. Optica, 2022, 9(2): 217-220.
[39] Liu S, Cui T J. Concepts, working principles, and applications of coding and programmable metamaterials[J]. Advanced Optical Materials, 2017, 5(22): 1700624.
[40] Li Z, Liu W W, Li Z C, et al. Tripling the capacity of optical vortices by nonlinear metasurface[J]. Laser & Photonics Reviews, 2018, 12(11): 1800164.
[41] Ma M L, Li Z, Liu W W, et al. Optical information multiplexing with nonlinear coding metasurfaces[J]. Laser & Photonics Reviews, 2019, 13(7): 1900045.
[42] Li G X, Zhang S, Zentgraf T. Nonlinear photonic metasurfaces [J]. Nature Reviews Materials, 2017, 2(5): 17010.
[43] Li Z, Liu W W, Geng G Z, et al. Multiplexed nondiffracting nonlinear metasurfaces[J]. Advanced Functional Materials, 2020, 30(23): 1910744.
[44] Hao Z L, Liu W W, Li Z C, et al. Full complex-amplitude modulation of second harmonic generation with nonlinear metasurfaces[J]. Laser & Photonics Reviews, 2021, 15(12): 2100207.
[45] Chen S M, Li G X, Cheah K W, et al. Controlling the phase of optical nonlinearity with plasmonic metasurfaces[J]. Nanophotonics, 2018, 7(6): 1313-1024.
[46] Jiang Y F, Liu W W, Li Z C, et al. Linear and nonlinear optical field manipulations with multifunctional chiral coding metasurfaces[J]. Advanced Optical Materials, 2023, 11(6): 2202186.
[47] Rodríguez-Fortuño F J, Espinosa-Soria A, Martínez A. Exploiting metamaterials, plasmonics and nanoantennas concepts in silicon photonics[J]. Journal of Optics, 2016, 18(12): 123001.
[48] Chen Y P, Yin Y, Ma L B, et al. Recent progress on optoplasmonic whispering-gallery-mode microcavities[J]. Advanced Optical Materials, 2021, 9(12): 2100143.
[49] Meng Y, Chen Y Z, Lu L H, et al. Optical meta-waveguides for integrated photonics and beyond[J]. Light, Science & Applications, 2021, 10(1): 235.
[50] Wang Z, Xiao Y H, Liao K, et al. Metasurface on integrated photonic platform: from mode converters to machine learning[J]. Nanophotonics, 2022, 11(16): 3531-3546.
[51] Yang Y, Seong J, Choi M, et al. Integrated metasurfaces for re-envisioning a near-future disruptive optical platform[J]. Light, Science & Applications, 2023, 12(1): 152.
[52] Guo R, Decker M, Staude I, et al. Bidirectional waveguide coupling with plasmonic Fano nanoantennas[J]. Applied Physics Letters, 2014, 105(5): 053114.
[53] Guo R, Decker M, Setzpfandt F, et al. High-bit rate ultra-compact light routing with mode-selective on-chip nanoantennas [J]. Science Advances, 2017, 3(7): e1700007.
[54] Meng Y, Liu Z T, Xie Z W, et al. Versatile on-chip light coupling and (de) multiplexing from arbitrary polarizations to controlled waveguide modes using an integrated dielectric metasurface[J]. Photonics Research, 2020, 8(4): 564-576.
[55] He T T, Meng Y, Liu Z T, et al. Guided mode meta-optics: metasurface-dressed waveguides for arbitrary mode couplers and on-chip OAM emitters with a configurable topological charge[J]. Optics Express, 2021, 29(24): 39406-39418.
[56] Wang Z, Li T T, Soman A, et al. On-chip wavefront shaping with dielectric metasurface[J]. Nature Communications, 2019, 10: 3547.
[57] Wang H W, Zhang Y, He Y, et al. Compact silicon waveguide mode converter employing dielectric metasurface structure[J]. Advanced Optical Materials, 2019, 7(4): 1801191.
[58] Xiang J L, Tao Z Y, Li X F, et al. Metamaterial-enabled arbitrary on-chip spatial mode manipulation[J]. Light, Science & Applications, 2022, 11(1): 168.
[59] Hao W M, Wang J, Chen L. Plasmonic metasurfaces enabled ultra-compact broadband waveguide TM-pass polarizer[J]. Annalen Der Physik, 2021, 533(1): 2000422.
[60] Wang C, Li Z Y, Kim M H, et al. Metasurface-assisted phase-matching-free second harmonic generation in lithium niobate waveguides[J]. Nature Communications, 2017, 8: 2098.
[61] Zhang Y, Shen J, Li J C, et al. High-speed electro-optic modulation in topological interface states of a one-dimensional lattice[J]. Light, Science & Applications, 2023, 12(1): 206.
[62] Yang R, Wan S, Shi Y Y, et al. Immersive tuning the guided waves for multifunctional on-chip metaoptics[J]. Laser & Photonics Reviews, 2022, 16(8): 2200127.
[63] Ha Y L, Guo Y H, Pu M B, et al. Monolithic-integrated multiplexed devices based on metasurface-driven guided waves [J]. Advanced Theory and Simulations, 2021, 4(2): 2000239.
[64] Zhou N, Zheng S, Cao X P, et al. Ultra-compact broadband polarization diversity orbital angular momentum generator with $3.6\times3.6\ \mu m^2$ footprint[J]. Science Advances, 2019, 5(5): eaau9593.
[65] Yulaev A, Zhu W Q, Zhang C, et al. Metasurface-integrated photonic platform for versatile free-space beam projection with polarization control[J]. ACS Photonics, 2019, 6(11): 2902-2909.
[66] Guo X X, Ding Y M, Chen X, et al. Molding free-space light with guided wave-driven metasurfaces[J]. Science Advances, 2020, 6(29): eabb4142.
[67] Cai L, Pan J Y, Hu S. Overview of the coupling methods used in whispering gallery mode resonator systems for sensing[J]. Optics and Lasers in Engineering, 2020, 127: 105968.

[68] Falek E, Katiyi A, Greenberg Y, et al. On-chip metasurface-on-facets for ultra-high transmission through waveguides in near-infrared[J]. Advanced Optical Materials, 2021, 9(11): 2100130.
[69] Siampour H, Kumar S, Davydov V A, et al. On-chip excitation of single germanium vacancies in nanodiamonds embedded in plasmonic waveguides[J]. Light: Science & Applications, 2018, 7: 61.
[70] Dolores-Calzadilla V, Romeira B, Pagliano F, et al. Waveguide-coupled nanopillar metal-cavity light-emitting diodes on silicon[J]. Nature Communications, 2017, 8: 14323.
[71] Meng Y, Hu F T, Shen Y J, et al. Ultracompact graphene-assisted tunable waveguide couplers with high directivity and mode selectivity[J]. Scientific Reports, 2018, 8: 13362.
[72] Vercruysse D, Neutens P, Lagae L, et al. Single asymmetric plasmonic antenna as a directional coupler to a dielectric waveguide[J]. ACS Photonics, 2017, 4(6): 1398-1402.
[73] Bernal Arango F, Kwadrin A, Koenderink A F. Plasmonic antennas hybridized with dielectric waveguides[J]. ACS Nano, 2012, 6(11): 10156-10167.
[74] Pors A, Nielsen M G, Bernardin T, et al. Efficient unidirectional polarization-controlled excitation of surface plasmon polaritons[J]. Light: Science & Applications, 2014, 3(8): e197.
[75] Pors A, Bozhevolnyi S I. Waveguide metacouplers for in-plane polarimetry[J]. Physical Review Applied, 2016, 5(6): 064015.
[76] Vahala K J. Optical microcavities[J]. Nature, 2003, 424(6950): 839-846.
[77] Doeleman H M, Verhagen E, Koenderink A F. Antenna-cavity hybrids: matching polar opposites for Purcell enhancements at any linewidth[J]. ACS Photonics, 2016, 3(10): 1943-1951.
[78] Ameling R, Giessen H. Microcavity plasmonics: strong coupling of photonic cavities and plasmons[J]. Laser & Photonics Reviews, 2013, 7(2): 141-169.
[79] Cognée K G, Doeleman H M, Lalanne P, et al. Cooperative interactions between nano-antennas in a high-*Q* cavity for unidirectional light sources[J]. Light, Science & Applications, 2019, 8: 115.
[80] Novotny L, van Hulst N. Antennas for light[J]. Nature Photonics, 2011, 5: 83-90.
[81] Staude I, Schilling J. Metamaterial-inspired silicon nanophotonics[J]. Nature Photonics, 2017, 11: 274-284.
[82] Guo Y H, Pu M B, Li X, et al. Chip-integrated geometric metasurface as a novel platform for directional coupling and polarization sorting by spin-orbit interaction[J]. IEEE Journal of Selected Topics in Quantum Electronics, 2018, 24(6): 4700107.
[83] Zhang Y B, Li Z C, Liu W W, et al. Spin-selective and wavelength-selective demultiplexing based on waveguide-integrated all-dielectric metasurfaces[J]. Advanced Optical Materials, 2019, 7(6): 1801273.
[84] Coles R J, Price D M, Dixon J E, et al. Chirality of nanophotonic waveguide with embedded quantum emitter for unidirectional spin transfer[J]. Nature Communications, 2016, 7: 11183.
[85] Zhang Y B, Li Z C, Liu W W, et al. Multi-band on-chip photonic spin Hall effect and selective excitation of whispering gallery modes with metasurface-integrated microcavity[J]. Optics Letters, 2021, 46(15): 3528-3531.
[86] Mueller J P B, Rubin N A, Devlin R C, et al. Metasurface polarization optics: independent phase control of arbitrary orthogonal states of polarization[J]. Physical Review Letters, 2017, 118(11): 113901.
[87] Meng Y, Hu F T, Liu Z T, et al. Chip-integrated metasurface for versatile and multi-wavelength control of light couplings with independent phase and arbitrary polarization[J]. Optics Express, 2019, 27(12): 16425-16439.
[88] Rubin N A, Zaidi A, Dorrah A H, et al. Jones matrix holography with metasurfaces[J]. Science Advances, 2021, 7(33): eabg7488.
[89] Ding Y H, Xu J, Da Ros F, et al. On-chip two-mode division multiplexing using tapered directional coupler-based mode multiplexer and demultiplexer[J]. Optics Express, 2013, 21(8): 10376-10382.
[90] Ohana D, Desiatov B, Mazurski N, et al. Dielectric metasurface as a platform for spatial mode conversion in nanoscale waveguides[J]. Nano Letters, 2016, 16(12): 7956-7961.
[91] 廖琨, 甘天奕, 胡小永, 等. 基于介质超表面的片上集成纳米光子器件[J]. 光学学报, 2021, 41(8): 0823001.
Liao K, Gan T Y, Hu X Y, et al. On-chip nanophotonic devices based on dielectric metasurfaces[J]. Acta Optica Sinica, 2021, 41(8): 0823001.
[92] Fan Y L, Le Roux X, Korovin A, et al. Integrated 2D-graded index plasmonic lens on a silicon waveguide for operation in the near infrared domain[J]. ACS Nano, 2017, 11(5): 4599-4605.
[93] Yao C H, Wang Z, Wang H W, et al. On-chip multi-mode manipulation via 2D refractive-index perturbation on a waveguide [J]. Advanced Optical Materials, 2020, 8(23): 2000996.
[94] Yao C N, Wang Y L, Zhang J H, et al. Dielectric nanoaperture metasurfaces in silicon waveguides for efficient and broadband mode conversion with an ultrasmall footprint[J]. Advanced Optical Materials, 2020, 8(17): 2000529.
[95] Guo J S, Ye C C, Liu C Y, et al. Ultra-compact and ultra-broadband guided-mode exchangers on silicon[J]. Laser & Photonics Reviews, 2020, 14(7): 2000058.
[96] Zhang Y, He Y, Wang H W, et al. Ultra-broadband mode size converter using on-chip metamaterial-based Luneburg lens[J]. ACS Photonics, 2021, 8(1): 202-208.
[97] Li Z Y, Kim M H, Wang C, et al. Controlling propagation and coupling of waveguide modes using phase-gradient metasurfaces [J]. Nature Nanotechnology, 2017, 12(7): 675-683.
[98] Wang R D, Wu Q, Cai W, et al. Broadband on-chip terahertz asymmetric waveguiding via phase-gradient metasurface[J]. ACS Photonics, 2019, 6(7): 1774-1779.
[99] Fan Y L, Cluzel B, Petit M, et al. 2D waveguided Bessel beam generated using integrated metasurface-based plasmonic axicon [J]. ACS Applied Materials & Interfaces, 2020, 12(18): 21114-21119.
[100] Deng L, Xu Y H, Jin R C, et al. On-demand mode conversion and wavefront shaping via on-chip metasurfaces[J]. Advanced Optical Materials, 2022, 10(23): 2200910.
[101] Wang Z J, Yao K, Chen M, et al. Manipulating smith-purcell emission with babinet metasurfaces[J]. Physical Review Letters, 2016, 117(15): 157401.
[102] Li L, Yao K, Wang Z J, et al. Harnessing evanescent waves by bianisotropic metasurfaces[J]. Laser & Photonics Reviews, 2020, 14(12): 1900244.
[103] Nikogosyan D N. Nonlinear optical crystals: a complete survey [M]. New York: Springer Science & Business Media, 2006.
[104] Boes A, Corcoran B, Chang L, et al. Status and potential of lithium niobate on insulator (LNOI) for photonic integrated circuits[J]. Laser & Photonics Reviews, 2018, 12(4): 1700256.
[105] Wang C, Zhang M, Chen X, et al. Integrated lithium niobate electro-optic modulators operating at CMOS-compatible voltages [J]. Nature, 2018, 562(7725): 101-104.
[106] He M B, Xu M Y, Ren Y X, et al. High-performance hybrid silicon and lithium niobate Mach-Zehnder modulators for 100 Gbit s^{-1} and beyond[J]. Nature Photonics, 2019, 13: 359-364.
[107] Li M X, Ling J W, He Y, et al. Lithium niobate photonic-crystal electro-optic modulator[J]. Nature Communications, 2020, 11: 4123.
[108] Chang L, Li Y F, Volet N, et al. Thin film wavelength converters for photonic integrated circuits[J]. Optica, 2016, 3(5): 531-535.
[109] Wang C, Langrock C, Marandi A, et al. Ultrahigh-efficiency

wavelength conversion in nanophotonic periodically poled lithium niobate waveguides[J]. Optica, 2018, 5(11): 1438-1441.
[110] Fang B, Li H M, Zhu S N, et al. Second-harmonic generation and manipulation in lithium niobate slab waveguides by grating metasurfaces[J]. Photonics Research, 2020, 8(8): 1296-1300.
[111] Krasnokutska I, Chapman R J, Tambasco J L J, et al. High coupling efficiency grating couplers on lithium niobate on insulator[J]. Optics Express, 2019, 27(13): 17681-17685.
[112] He L Y, Zhang M, Shams-Ansari A, et al. Low-loss fiber-to-chip interface for lithium niobate photonic integrated circuits[J]. Optics Letters, 2019, 44(9): 2314-2317.
[113] Ding Y M, Chen X, Duan Y, et al. Metasurface-dressed two-dimensional on-chip waveguide for free-space light field manipulation[J]. ACS Photonics, 2022, 9(2): 398-404.
[114] Tachella J, Altmann Y, Mellado N, et al. Real-time 3D reconstruction from single-photon lidar data using plug-and-play point cloud denoisers[J]. Nature Communications, 2019, 10: 4984.
[115] Reutebuch S E, Andersen H E, McGaughey R J. Light detection and ranging (LIDAR): an emerging tool for multiple resource inventory[J]. Journal of Forestry, 2005, 103(6): 286-292.
[116] Levola T. Diffractive optics for virtual reality displays[J]. Journal of the Society for Information Display, 2006, 14(5): 467-475.
[117] Liu Z Y, Wang D Y, Gao H, et al. Metasurface-enabled augmented reality display: a review[J]. Advanced Photonics, 2023, 5(3): 034001.
[118] Fang B, Wang Z Z, Gao S L, et al. Manipulating guided wave radiation with integrated geometric metasurface[J]. Nanophotonics, 2022, 11(9): 1923-1930.
[119] Hsieh P Y, Fang S L, Lin Y S, et al. Integrated metasurfaces on silicon photonics for emission shaping and holographic projection[J]. Nanophotonics, 2022, 11(21): 4687-4695.
[120] 杨睿, 于千茜, 潘一苇, 等. 基于片上超表面的多路方向复用全息术[J]. 光电工程, 2022, 49(10): 220177.
Yang R, Yu Q Q, Pan Y W, et al. Directional-multiplexing holography by on-chip metasurface[J]. Opto-Electronic Engineering, 2022, 49(10): 220177.
[121] Cognée K G, Doeleman H M, Lalanne P, et al. Generation of pure OAM beams with a single state of polarization by antenna-decorated microdisk resonators[J]. ACS Photonics, 2020, 7(11): 3049-3060.
[122] Zhang Y B, Li Z C, Liu W W, et al. On-chip multidimensional manipulation of far-field radiation with guided wave-driven metasurfaces[J]. Laser & Photonics Reviews, 2023, 17(9): 2300109.
[123] Huang H Q, Overvig A C, Xu Y, et al. Leaky-wave metasurfaces for integrated photonics[J]. Nature Nanotechnology, 2023, 18(6): 580-588.
[124] Xu G Y, Overvig A, Kasahara Y, et al. Arbitrary aperture synthesis with nonlocal leaky-wave metasurface antennas[J]. Nature Communications, 2023, 14: 4380.
[125] Ji J T, Wang Z Z, Sun J C, et al. Metasurface-enabled on-chip manipulation of higher-order poincaré sphere beams[J]. Nano Letters, 2023, 23(7): 2750-2757.
[126] Shi Y Y, Wan C W, Dai C J, et al. Augmented reality enabled by on-chip meta-holography multiplexing[J]. Laser & Photonics Reviews, 2022, 16(6): 2100638.
[127] Shi Y Y, Wan C W, Dai C J, et al. On-chip meta-optics for semi-transparent screen display in sync with AR projection[J]. Optica, 2022, 9(6): 670-676.
[128] Fang B, Shu F Z, Wang Z Z, et al. On-chip non-uniform geometric metasurface for multi-channel wavefront manipulations [J]. Optics Letters, 2023, 48(11): 3119-3122.
[129] Wu C M, Yu H S, Lee S, et al. Programmable phase-change metasurfaces on waveguides for multimode photonic convolutional neural network[J]. Nature Communications, 2021, 12: 96.
[130] Chen B G, Bruck R, Traviss D, et al. Hybrid photon-plasmon coupling and ultrafast control of nanoantennas on a silicon photonic chip[J]. Nano Letters, 2018, 18(1): 610-617.
[131] Kang M, Liu T, Chan C T, et al. Applications of bound states in the continuum in photonics[J]. Nature Reviews Physics, 2023, 5: 659-678.
[132] Zou C L, Cui J M, Sun F W, et al. Guiding light through optical bound states in the continuum for ultrahigh-*Q* microresonators[J]. Laser & Photonics Reviews, 2015, 9(1): 114-119.
[133] Zeng Y X, Hu G W, Liu K P, et al. Dynamics of topological polarization singularity in momentum space[J]. Physical Review Letters, 2021, 127(17): 176101.
[134] Chang L, Jiang X S, Hua S Y, et al. Parity-time symmetry and variable optical isolation in active-passive-coupled microresonators[J]. Nature Photonics, 2014, 8: 524-529.
[135] Feng L, El-Ganainy R, Ge L. Non-Hermitian photonics based on parity-time symmetry[J]. Nature Photonics, 2017, 11: 752-762.
[136] Özdemir Ş K, Rotter S, Nori F, et al. Parity-time symmetry and exceptional points in photonics[J]. Nature Materials, 2019, 18(8): 783-798.
[137] Miri M A, Alù A. Exceptional points in optics and photonics[J]. Science, 2019, 363(6422): eaar7709.
[138] Yin X F, Inoue T, Peng C, et al. Topological unidirectional guided resonances emerged from interband coupling[J]. Physical Review Letters, 2023, 130(5): 056401.
[139] Li Q T, van de Groep J, White A K, et al. Metasurface optofluidics for dynamic control of light fields[J]. Nature Nanotechnology, 2022, 17(10): 1097-1103.
[140] Kühner L, Sortino L, Berté R, et al. Radial bound states in the continuum for polarization-invariant nanophotonics[J]. Nature Communications, 2022, 13: 4992.
[141] Li Z, Zhang X Y, Ma R D, et al. Versatile optical manipulation of trions, dark excitons and biexcitons through contrasting exciton-photon coupling[J]. Light, Science & Applications, 2023, 12(1): 295.
[142] Vazimali M G, Fathpour S. Applications of thin-film lithium niobate in nonlinear integrated photonics[J]. Advanced Photonics, 2022, 4(3): 034001.
[143] Yang L C, Li G R, Gao X M, et al. Topological-cavity surface-emitting laser[J]. Nature Photonics, 2022, 16: 279-283.
[144] Lin J T, Farajollahi S, Fang Z W, et al. Electro-optic tuning of a single-frequency ultranarrow linewidth microdisk laser[J]. Advanced Photonics, 2022, 4(3): 036001.
[145] El-Ganainy R, Makris K G, Khajavikhan M, et al. Non-Hermitian physics and PT symmetry[J]. Nature Physics, 2018, 14: 11-19.
[146] Yu S W, Li Z C, Liu W W, et al. Tunable dual-band and high-quality-factor perfect absorption based on VO_2-assisted metasurfaces[J]. Optics Express, 2021, 29(20): 31488-31498.
[147] Wang Q, Rogers E T F, Gholipour B, et al. Optically reconfigurable metasurfaces and photonic devices based on phase change materials[J]. Nature Photonics, 2016, 10: 60-65.
[148] Ma W, Liu Z C, Kudyshev Z A, et al. Deep learning for the design of photonic structures[J]. Nature Photonics, 2021, 15: 77-90.
[149] Ma W, Hou M J, Luo R Q, et al. Topologically-optimized on-chip metamaterials for ultra-short-range light focusing and mode-size conversion[J]. Nanophotonics, 2023, 12(6): 1189-1197.
[150] Piggott A Y, Lu J, Lagoudakis K G, et al. Inverse design and demonstration of a compact and broadband on-chip wavelength demultiplexer[J]. Nature Photonics, 2015, 9: 374-377.
[151] Jia H, Zhou T, Fu X, et al. Inverse-design and demonstration of ultracompact silicon meta-structure mode exchange device[J]. ACS Photonics, 2018, 5(5): 1833-1838.

[152] Molesky S, Lin Z, Piggott A Y, et al. Inverse design in nanophotonics[J]. Nature Photonics, 2018, 12: 659-670.
[153] Wang K Y, Ren X S, Chang W J, et al. Inverse design of digital nanophotonic devices using the adjoint method[J]. Photonics Research, 2020, 8(4): 528-533.
[154] 玛地娜, 程化, 田建国, 等. 人工光子学器件的逆向设计方法与应用(特邀)[J]. 光子学报, 2022, 51(1): 0151110.
Ma D N, Cheng H, Tian J G, et al. Inverse design methods and applications of photonics devices (invited)[J]. Acta Photonica Sinica, 2022, 51(1): 0151110.
[155] Liu Y, Shi Y Y, Wang Z J, et al. On-chip integrated metasystem with inverse-design wavelength demultiplexing for augmented reality[J]. ACS Photonics, 2023, 10(5): 1268-1274.
[156] Zhou H Y, Liao K, Su Z X, et al. Tunable on-chip mode converter enabled by inverse design[J]. Nanophotonics, 2023, 12(6): 1105-1114.

Light Field Manipulation Based on On-Chip Integrated Artificial Microstructures (Invited)

Wang Yanchun[1], Zhang Yuebian[1*], Cheng Hua[1**], Chen Shuqi[1,2***]

[1]*The Key Laboratory of Weak Light Nonlinear Photonics, Ministry of Education, School of Physics and TEDA Institute of Applied Physics, Nankai University, Tianjin* 300071, *China*;

[2]*Collaborative Innovation Center of Extreme Optics, Shanxi University, Taiyuan* 030006, *Shanxi, China*

Abstract

Significance Light is an indispensable carrier of energy and information in humans' daily life. The main information of light fields can be described by a few attributes such as amplitude, phase, frequency, and polarization. How to flexibly and effectively manipulate these light field dimensions has been a key research focus in optics and photonics. Meanwhile, with the development of technology, "Moore's Law" is gradually losing its effectiveness, and traditional electronic chips are facing increasing performance improvement challenges. Compared with electrons, photons have fast transmission velocity, high information-carrying capacity, and unique parallel processing capability. Therefore, replacing electronic components partially or completely with optical components is expected to solve many problems facing traditional electronic chips. However, traditional optical components are generally large in size and heavy. Therefore, the miniaturization and integration of multiple optical components into the same chip is an important trend in the future development of photonic chips.

Optical artificial microstructure (also called "metaatom") is a kind of artificial structure with subwavelength size in one or more dimensions, which can resonate with light fields to achieve functions beyond traditional natural materials. A metasurface can be formed by ordering optical artificial microstructures on a two-dimensional surface. It provides not only practical and effective solutions for the miniaturization and integration of traditional optical components but also more diverse means of controlling light fields and richer light-matter interactions. However, most current metasurfaces are focused on the manipulation of free-space light fields, and a metasurface can only achieve a single or a few functions. To further achieve more compact and versatile photonic chips, researchers have begun to integrate optical artificial microstructures with on-chip optical waveguides or optical microcavities in recent years. The research on on-chip integrated artificial microstructures injects new vitality into light field manipulation and nano-photonics devices. Thanks to their subwavelength sizes and unique resonance characteristics, artificial microstructures can serve as a bridge connecting free-space light fields with on-chip waveguide modes, thus opening up new opportunities for fully manipulating light in integrated optical systems and free space. Even though various novel optical devices have been proposed based on on-chip integrated artificial microstructures in the past few years, they still face a series of challenges in large-scale ultra-compact integration and performance improvement. Therefore, a review of light field manipulation based on on-chip integrated artificial microstructures is necessary to provide helpful guidance for researchers to design novel on-chip optical devices.

Progress Based on different types of light fields manipulated by on-chip integrated artificial microstructures, we categorize them into three classes for discussions (Fig. 1). The first category involves "meta-couplers" that can couple free-space optical modes into waveguides or microcavities and convert them into specific guided modes. The artificial microstructure-based meta-couplers can achieve more diverse and complex functions than traditional grating couplers, such as wavelength- and polarization-demultiplexing, or the excitation of specific guided modes (Fig. 2). The second category involves "in-plane modulators" that enable on-chip manipulation of confined light fields within the chip plane. Artificial microstructures can be either partially- or fully-etched aperture antennas, or they can be directly integrated onto the

waveguide surface. By adopting the refractive index perturbation or phase gradient provided by the microstructures, in-plane focusing of waveguide modes, filters, mode conversions between different guided modes, and on-chip nonlinear harmonic generations can be achieved (Figs. 3 and 4). Additionally, on-chip integrated artificial microstructures can be combined with dynamic control schemes such as electro-optic modulators to further optimize the modulator's footprint and bandwidth performance. The third category involves "guided wave-driven metasurfaces" that can convert guided waves into free-space waves. By employing one-dimensional (Fig. 5) and multi-dimensional (Figs. 6 and 7) manipulation of far-field radiation, guided wave-driven metasurfaces can achieve various applications, such as holographic imaging, vortex beam generation, beam focusing, and beam deflection. Theoretically, the polarization, amplitude, phase, and orbital angular momentum of the emitted light field can be manipulated arbitrarily to provide new solutions for applications such as virtual reality, augmented reality, and information encryption and multiplexing.

Conclusions and Prospects We systematically introduce the research progress of on-chip integrated artificial microstructures in the areas of free-space light coupling, in-plane manipulation of guided modes, and the manipulation of off-chip radiated fields. Additionally, we provide an outlook on some emerging directions in this field. By cascading multiple optical metasurfaces on waveguides, on-chip optical components can be more compact, and multifunctional devices beyond traditional metasurfaces can be realized. Some novel physical effects such as bound states in the continuum, parity-time symmetry, and exceptional points can provide a richer range of physical processes for on-chip integrated artificial microstructures. The introduction of new materials such as two-dimensional materials and laser gain materials can provide a new platform for studying excitons, valley spin, nonlinear effects, on-chip lasing, and other phenomena. The utilization of inverse design methods such as deep learning and topological optimization can serve as powerful tools for designing on-chip integrated artificial microstructures. In summary, with the advancement of technology, the application scope of on-chip integrated artificial microstructures will become more widespread. The operating wavelength range can expand from visible and near-infrared light to terahertz, microwave, and ultraviolet wavebands. Additionally, numerous miniaturized and integrated on-chip photonic devices will continue to emerge with the help of artificial microstructures.

Key words artificial microstructure; metasurface; light field manipulation; integrated optics; micro-nano optics